Theoretical study on the electronic spectrum of TcO_4^-

J. Hasegawa, K. Toyota, M. Hada, H. Nakai, H. Nakatsuji*

Department of Synthetic Chemistry and Biological Chemistry, Faculty of Engineering,
Kyoto University, Sakyo-ku, Kyoto, 606-01, Japan, Fax: 81-75-753-5910

Summary. The theoretical electronic spectrum of TcO_4^- calculated by the SAC(symmetry adapted cluster)/SAC-CI method is presented. The spectrum is in good agreement with the experimental one. The observed peaks are assigned and the existence of several absorptions in the energy region higher than that observed is predicted. The difference and the similarity between the electronic spectra of TcO_4^- and MnO_4^- are clarified. The spectral difference between TcO_4^- and MnO_4^- is due to a remarkably high energy shift of the 3^1T_2 state of TcO_4^-.

1 Introduction

Four coordinated oxo-metal complexes are important as oxidizing agents. Their visible and ultraviolet spectra have been reported [1], and theoretical assignments [2] were attempted by Ziegler et al. in 1976. Some complexes show interesting photochemistry as observed for MnO_4^- [3, 4]. We have studied the electronic spectra of the tetraoxo metal complexes, CrO_4^{2-} [5], MoO_4^{2-} [6], MnO_4^- [7], RuO_4 [8], OsO_4 [8], and also CrO_2Cl_2 [9] by the SAC (symmetry adapted cluster) [10] and the SAC-CI (symmetry adapted cluster-configuration interaction) [11] method [12]. We have investigated the similarity and the difference in the electronic spectra of these tetraoxo metal complexes [5]. It has been shown that a sufficient inclusion of electron correlations for both ground and excited states are important for reliable *ab initio* assignments of the spectra.

Technetium belongs to the group VIIA metal as manganese and TcO_4^- is also a strong oxidizing reagent [13]. However, the electronic spectrum[14] of TcO_4^- shown in Fig. 1 is very different from that of MnO_4^-. The peaks of TcO_4^- lie in a higher energy region than those of MnO_4^-. TcO_4^- does not have a broad band like that of MnO_4^- at 3.47 eV, and the energy separation between Bands I and II in MnO_4^- is larger than that of TcO_4^-. The correspondence between the Band III's of these compounds is unclear.

---

* *Present address:* Institute for Fundamental Chemistry, 34-4 Takano Nishi-Hiraki-cho, Sakyo-ku, Kyoto, 606, Japan
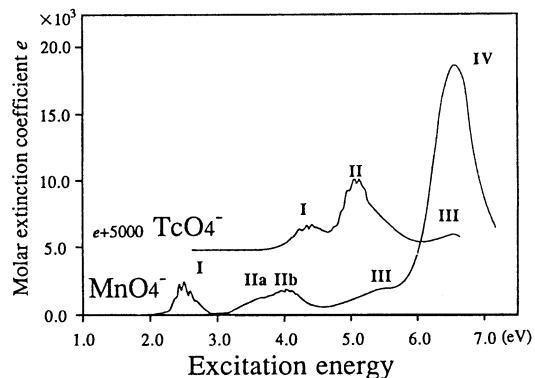
Fig. 1. Electronic absorption spectra of TcO_4^- and MnO_4^- in the vapor phase, see Ref. [14]

Table 1. Dimensions of the SAC/SAC-CI calculations of TcO_4^-

Symmetry	After selection	Before selection
Ground state: SAC		
$^1A_1$	3686	23809
Excited state[a]: SAC-CI		
$^1A_1$	7444	23809
$^1A_2$	6676	23280
$^1B_1$	7191	23436

[a] $^1B_2$ states are degenerate with $^1B_1$ states in the tetrahedral symmetry

In this study, we calculate the ground and excited states of TcO_4^- by the SAC/SAC-CI theory and present a theoretical assignment of the observed spectrum and a prediction of the peaks so far not observed. We analyze the bonding nature of the ground and excited states and compare the natures of the excited states with those of the other oxo-metal complexes studied previously [5–9].

2 Computational details

The geometry of TcO_4^- is fixed to the T_d symmetry with the Tc–O bond distance of 1.71 Å adopted from the experimental data of X-ray crystallography [15].

The Gaussian basis set we use in this work is valence DZ and TZ levels. We use for Tc the $(16s10p7d)/[7s3p3d]$ set [16] and the two polarization p-functions with the exponents $\alpha = 0.028$ and 0.086 [16], and for O the $(9s5p)/[4s2p]$ set [16]. From our experience [5–9], this basis set would reliably describe the valence excited states of this molecule.

The HF orbitals calculated by the HONDO program [17] are used as reference orbitals. Electron correlations in the ground state are treated by the SAC [10] method and those in the excited states by the SAC-CI method [11] with the use of the program SAC85 [18]. The space of the active orbitals must be sufficiently large to accurately describe the valence excitations. The active space of the present SAC/SAC-CI calculations consists of 12 higher occupied orbitals and 36 lower unoccupied orbitals: all valence-type occupied and unoccupied orbitals are included. For the linked term, all single excitations and double excitations selected

by the perturbative method [19] are included. The main configurations whose coefficients are larger than 0.1 in the 12 lower solutions in preliminary SE-CI calculations in each symmetry are used as the reference configurations for the perturbation selection [19]. The energy thresholds $\lambda g = 4.0 \times 10^{-5}$ Hartree for the ground state and $\lambda_e = 7.0 \times 10^{-5}$ Hartree for the excited states are used in the present calculation. The numbers of the linked configurations are shown in Table 1.

3 Results and discussions

3.1 Ground state of TcO_4^-

The SCF orbital sequence and the orbital characters are shown in Table 2. The plus (+) and minus (−) signs denote the bonding and antibonding combinations, respectively. The lowest three valence orbitals $1e$, $1t_2$, and $1a_1$ are the bonding MOs between the $4d$ orbitals of Tc and the $2p$ orbitals of O. The higher occupied orbitals $2t_2$ and $1t_1$ are nonbonding MOs mainly composed of the oxygen $2p$ orbitals. In particular, the highest occupied MO (HOMO) $1t_1$ is completely localized on oxygens. The lowest unoccupied MO (LUMO) $2e$ and the higher unoccupied $4t_2$ MO are antibonding between the Tc $4d$ and the O $2p$ orbitals. These antibonding MOs have larger amplitudes on Tc than on O. The unoccupied $2a_1$ and $3t_2$ MOs are the nonbonding MOs mainly composed of the Tc $5s$ and $5p$ orbitals, respectively.

Comparing with RuO_4 [8] and MoO_4^{2-} [6], which are isoelectronic with TcO_4^-, orbital energies of the valence occupied MOs are shifted by about $+ 7.5$ and $- 8.0$ eV, respectively. Further, the energy shifts are larger for the bonding orbitals than for the ligand orbitals by about 1 eV. The bonding MOs having larger amplitudes on the metal than the ligand MOs feel the change of the nuclear charge more sensitively.

Table 3 shows the total energies, Mulliken atomic orbital populations and net charges of TcO_4^- calculated by the HF and SAC methods. By including electron

Table 2. HF orbital energies and characters

Symmetry	Character[a]		Orbital energy [eV]
Occupied orbitals			
$1e$	$Tc(4d) + O(2p)$	:B	− 12.92
$1t_2$	$Tc(4d) + O(2p)$	:B	− 12.84
$1a_1$	$Tc(4d) + O(2p)$	:B	− 8.66
$2t_2$	$O(2p)$	:L	− 8.60
$1t_1$	$O(2p)$	:L	− 7.77
Unoccupied orbitals			
$2e$	$Tc(4d) − O(2p)$	:A	4.62
$2a_1$	$Tc(5s)$	:M	5.65
$3t_2$	$Tc(5p)$	:M	5.70
$4t_2$	$Tc(4d) − O(2p)$	:A	7.35

[a] (+) and (−) denote bonding and antibonding combinations, respectively. B, A, L, and M mean bonding, antibonding, ligand and metal orbitals, respectively

Table 3. Total energy and the valence electron population for the ground state of TcO_4^-

Method	Energy [Hartree]	Tc				O		
		$5s$	$5p$	$4d$	Charge	$2s$	$2p$	Charge
HF	-4500.66022	0.032	0.310	4.755	$+1.800$	1.968	4.737	-0.700
SAC	-4501.15316	0.035	0.361	5.013	$+1.487$	1.967	4.660	-0.622
Δ^a	-0.49294	$+0.003$	$+0.051$	$+0.258$	-0.313	-0.001	-0.077	$+0.078$

^{a} The difference between HF and SAC values

Table 4. Occupation numbers of the HF orbitals and the SAC natural orbitals for the ground state of TcO_4^-

Orbital	HF	SAC	Difference	(Per MO)
Occupied orbitals				
$1e$	4.0	3.9542	-0.0458	-0.0229
$1t_2$	6.0	5.9240	-0.0760	-0.0253
$1a_1$	2.0	1.9688	-0.0312	-0.0312
$2t_2$	6.0	5.9029	-0.0971	-0.0324
$1t_1$	6.0	5.8961	-0.1039	-0.0346
Unoccupied orbitals				
$2e$	0.0	0.1237	$+0.1237$	$+0.0619$
$2a_1$	0.0	0.0494	$+0.0494$	$+0.0494$
$3t_2$	0.0	0.1078	$+0.1078$	$+0.0359$
$4t_2$	0.0	0.0252	$+0.0252$	$+0.0084$

correlations, the ionicity of the Tc–O bond is much relaxed, and the relaxation is largest on the Tc $4d$ orbitals. Table 4 shows the occupation numbers of the natural orbitals of the SAC wave function. In comparison with the HF ones, the occupations of the $1t_1$ and $2t_2$ MOs decrease more than those of the other occupied orbitals. In the unoccupied MOs, the occupancies of the $2e$ and $2a_1$ MOs increase by including electron correlations. These changes in the occupation numbers result in an increase of the Tc $4d$ occupations and a decrease of the O $2p$ occupations as shown in Table III. Similar relaxation was also found in our previous studies on MnO_4^-, CrO_4^{2-}, etc. [5–9], so this phenomenon seems to be quite general.

3.2 Excited states of TcO_4^-

Figure 1 shows the experimental electronic spectrum of TcO_4^- together with that of the related complex, MnO_4^- [14]. In the spectrum of TcO_4^-, there are two strong peaks at 4.27 and 5.00 eV (Bands I and II) and a weak peak at 6.59 eV (Band III). These peaks would be due to the allowed transitions. As compared with the electronic spectrum of MnO_4^-, (1) the peaks of TcO_4^- shift entirely to the higher energy region, (2) Bands I and II are different from those of MnO_4^- in both the energy splitting and intensity, (3) in MnO_4^-, Bands IIa and IIb are due to the different excited states [7], but in TcO_4^- we do not know how many states there are in Band II, and (4) the strong peak of MnO_4^- at 6.5 eV is not observed for TcO_4^- in the observed energy region.

We summarize in Table 5 the SAC/SAC-CI results for the singlet excitation energy, oscillator strength, and the net charges on Tc and O. In the T_d symmetry only the transitions to the $^1T_2$ states are dipole-allowed. The SAC/SAC-CI theoretical spectrum for TcO$_4^-$ is shown in Fig. 2 and compared with the experimental spectrum. The theoretical spectrum reproduces well the excitation energies and the intensities of the observed peaks in the 4–6 eV region. From Table 5 the excited states in TcO$_4^-$ may be divided into two regions (Regions A and B). Region A is 3.0–7.2 eV and Region B is above Region A. The 1–3 $^1T_2$ states in Region A are characterized as the transitions from the ligand to the antibonding MOs and 4–6 $^1T_2$ states in Region B as the transitions from the ligand to the metal. Although all the states are the charge transfer states from O to Tc, the amount of transferred charge is larger in Region B than in Region A. This trend is similar to that in MnO$_4^-$.

Next we discuss more details of the absorptions. Based on the present calculation, the observed Bands I, II, and III are assigned to 1^1T_2, 2^1T_2, and 3^1T_2 states, respectively, by comparing the experimental and theoretical spectra in both the excitation energy and the intensity. This assignment is the same as that by Ziegler et al. [2] with the Hartree–Fock–Slater discrete variational method.

Band I corresponds to the first dipole-allowed excited state 1^1T_2 ($1t_2 \rightarrow 2e$), and the fine structure spacing of about 0.1 eV represents the vibrational structure in

Table 5. Ground and excited states of TcO$_4^-$

State	Main configuration ($C \geqslant 0.3$)	Nature[a]	Excitation energy e(V) Exptl.	SAC-CI	Oscillator strength Exptl.	SAC-CI	Net charge Tc	O
XA$_1$	1.00(HF)			0.00			− 1.486	− 0.622
1T$_1$	0.96($1t_1 \rightarrow 2c$)	L → A		3.83		Forbidden	+ 1.283	− 0.571
1T$_2$	0.77($1t_1 \rightarrow 2e$)	L → A	4.27	4.28	Middle	0.0171	+ 1.293	− 0.573
	0.57($2t_2 \rightarrow 2e$)	L → A						
2T$_1$	0.95($2t_2 \rightarrow 2e$)	L → A		4.61		Forbidden	+ 1.319	− 0.580
1E	0.96($1a_1 \rightarrow 2e$)	B → A		4.98		Forbidden	+ 1.305	− 0.576
2T$_2$	0.71($2t_2 \rightarrow 2e$)	L → A	5.00	5.29	Strong	0.0415	+ 1.315	− 0.579
2E	0.67($1t_1 \rightarrow 4t_2$)	L → A		6.08		Forbidden	+ 1.268	− 0.567
3T$_2$	0.55($1t_1 \rightarrow 4t_2$)	L → A	6.59	6.20	Weak	0.0025	+ 1.259	− 0.564
3T$_1$	0.57($1t_1 \rightarrow 4t_2$)	L → A		6.42		Forbidden	+ 1.227	− 0.557
1A$_2$	0.48($1t_1 \rightarrow 4t_2$)	L → A		6.54		Forbidden	+ 1.237	− 0.559
4T$_1$	0.85($1t_1 \rightarrow 2a_1$)	L → M		6.95		Forbidden	+ 0.657	− 0.414
1A$_1$	0.48($2t_2 \rightarrow 4t_2$)	L → A		7.03		Forbidden	+ 1.274	− 0.569
5T$_1$	0.56($2t_2 \rightarrow 4t_2$)	L → A		7.10		Forbidden	+ 1.213	− 0.553
3E	0.66($2t_2 \rightarrow 4t_2$)	L → A		7.19		0.0000	+ 1.249	− 0.562
4T$_2$	0.39($2t_2 \rightarrow 4t_2$)	L → A		7.45		0.0000	+ 1.042	− 0.510
	0.37($1a_1 \rightarrow 4t_2$)	B → A						
	0.34($2t_2 \rightarrow 2a_1$)	L → M						
	0.32($1t_1 \rightarrow 3t_2$)	L → M						
5T$_2$	0.58($2t_2 \rightarrow 2a_1$)	L → M		7.56		0.0046	+ 0.858	− 0.465
	0.42($1a_1 \rightarrow 4t_2$)	B → A						
2A$_1$	0.85($1a_1 \rightarrow 2a_1$)	B → M		8.18		Forbidden	+ 0.608	− 0.402
6T$_2$	0.67($2t_2 \rightarrow 2a_1$)	L → M		8.19		0.0339	+ 0.623	− 0.406

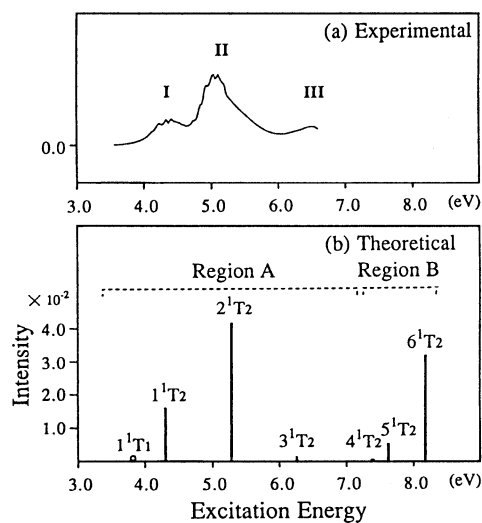[a] B, A, L, and M denote bonding, antibonding, ligand and metal orbitals, respectively

Fig. 2. (a) Experimental and (b) theoretical spectra of TcO_4^-. Experimental spectrum is due to Mullen et al., see Ref. [14]. The optically forbidden state is indicated by an open circle
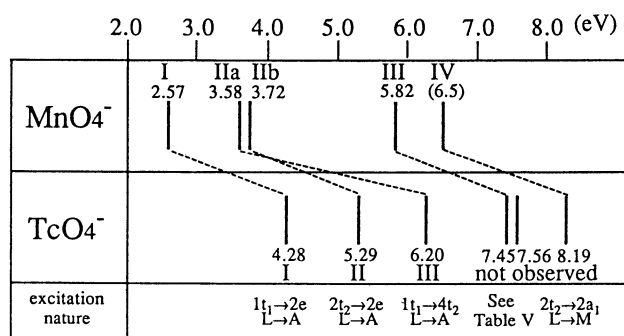

Fig. 3. Comparison of the calculated excitation energies for optically allowed $^1T_2$ states of MnO_4^- and TcO_4^-. For MnO_4^-, see Ref. [7]

the excited state. The first observed peak of MnO_4^- has the same nature as that of TcO_4^-, as seen from the corresponding diagram given in Fig. 3.

Bands II and III are due to the allowed states of 2^1T_2 $(2t_2 \rightarrow 2e)$ and 3^1T_2 $(1t_1 \rightarrow 4t_2)$, respectively. This assignment is different from that for MnO_4^-, since, in MnO_4^-, the 2^1T_2 and 3^1T_2 states constitute Band II [7]. In Fig. 1, Band II of MnO_4^- is thus divided into Bands IIa and IIb. Furthermore, the natures of Bands II and III of TcO_4^- are just the reverse of those of Bands IIa and IIb of MnO_4^-, as shown in the corresponding diagram in Fig. 3.

state MnO_4^- TcO_4^-

2^1T_2 ↔ Band IIb ↔ Band II

3^1T_2 ↔ Band IIa ↔ Band III
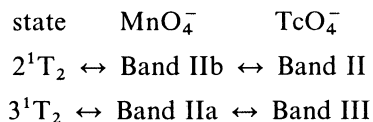
The existence of the vibrational structure in Band IIb of MnO_4^- is consistent with that of Band II of TcO_4^-. The energy separation between Bands II and III in TcO_4^- is much larger than that between Bands IIa and IIb in MnO_4^-, although the corresponding excited states have similar nature. It is due to a remarkably high energy shift of the 3^1T_2 states $(1t_1 \rightarrow 4t_2)$ in TcO_4^-, and this shift is easily explained from the orbital energy levels shown in Fig. 4. The orbital energy difference
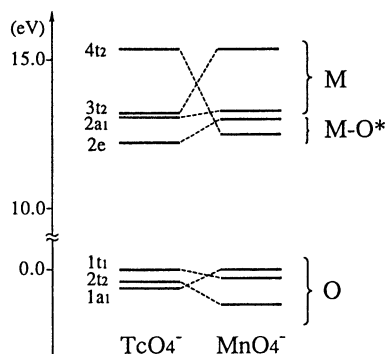
Fig. 4. Orbital energy levels of TcO_4^- and MnO_4^- with their HOMOs as the reference level. The MOs having the same nature are connected by the dotted line

between the $1t_1$ and $4t_2$ MOs in TcO_4^- is much larger than that in MnO_4^-. The $4t_2$ MO of TcO_4^- lies in high energy, since the anti-bonding interaction between metal and ligand is larger in TcO_4^- than in MnO_4^-. This is because the Tc $4d$ orbital is more diffuse than the Mn $3d$ orbital and then the metal–ligand overlap interaction is larger in TcO_4^- than in MnO_4^-.

In the previous study on the photochemical decomposition reaction of MnO_4^- [4], 1^1T_2 and 3^1T_2 states are shown to play important roles. Although no report for the photoreaction of TcO_4^- is found, the 1^1T_2 and 2^1T_2 states are expected to be important as photochemical reaction channels since, in TcO_4^-, these states correspond to the 1^1T_2 and 3^1T_2 states of MnO_4^-.

For the energy region higher than Band III, there are no experimental data for the electronic absorption of TcO_4^-. However, as seen from Table 5, we can predict an existence of the three dipole-allowed electronic states 4^1T_2, 5^1T_2, and 6^1T_2, whose excitation energies are calculated at 7.45, 7.56, and 8.19 eV, respectively, and the intensities to be weak, weak, and strong, respectively. The 4^1T_2 state has a mixed nature of L → A and L → M transitions, and the intensity is low. The 5^1T_2 and 6^1T_2 states originate from the L to M ($2t_2 \rightarrow 2a_1$) excitation, and so a larger amount of electronic charge on O is transferred to the metal than in the $1-4^1T_2$ states in Region A as seen from Table 5. The 4^1T_2 state lies just on the border of Regions A and B since, as seen from Table 5, the nature of the transition switches from L → A to L → M on this state and the amount of charge transferred from ligand to metal is median between those in Regions A and B.

The peaks of the 5^1T_2 and 6^1T_2 states calculated at 7.45 and 7.56 eV for TcO_4^- would correspond to the peak III of MnO_4^- shown in Fig. 1. In particular, the 6^1T_2 state of TcO_4^- has a large intensity of 0.0339 so that it would correspond to the strong peak (Band IV) observed at 6.5 eV for MnO_4^- (Fig. 1). In comparison with our previous results for CrO_4^{2-} [5], the 6^1T_2 state of TcO_4^- has the same character as the 5^1T_2 state of CrO_4^{2-}, which gives a strong peak at 6.0–7.0 eV [20]. The $4-6^1T_2$ states may lie higher than the first ionization potential, since they are excitations from the orbitals lower than $1t_1$ (HOMO). Thus, we propose to examine a new band system in the higher energy region (7.5–8.0 eV) of the TcO_4^- spectrum.

In the electronic spectra of $LiMnO_4 \cdot 3H_2O$ and $Ba(MnO_4)_2 \cdot 3H_2O$, a weak absorption called "Teltow band" was observed [21] in the red side of the 1^1T_2 state. This band was calculated to be a symmetry forbidden 1^1T_1 state in our previous work [5, 7]. This state can be observed by a symmetry lowering from T_d to C_{3v} in its crystal. For TcO_4^-, the 1^1T_1 state is calculated at 3.83 eV and has

the same nature as the symmetry allowed $1\,^1T_2$ state calculated at 4.28 eV (Band I), the excitation from ligand to antibonding MO ($2t_1 \rightarrow 2e$). In this class of complexes like MnO_4^-, CrO_4^-, and so forth, the $1\,^1T_1$ and $1\,^1T_2$ states originate from the same MO excitations and the $1\,^1T_1$ state is always at the red side of the $1\,^1T_2$ state, although the energy itself is different for different complexes. The energy difference between the $1\,^1T_1$ and $1\,^1T_2$ states is roughly due to the difference in the exchange integrals.

Compared with MnO_4^-, all the peaks observed for TcO_4^- are shifted to the higher energy region by 1.5–2.6 eV as seen from Fig. 3. This is roughly explained as follows [5]. In the frozen orbital approximation, the HF excitation energy may be expressed as

$$\Delta E_{i \rightarrow a} = \varepsilon_a - \varepsilon_i - J_{ia} + 2K_{ia}.$$

Because the transitions are from ligand to metal, the transitions are affected by the metal–ligand bond length. Since the Tc–O bond is longer than the Mn–O bond, the J_{ia} values of TcO_4^- should be smaller than those of MnO_4^-.

4 Conclusion

In this study, we have applied the SAC/SAC-CI method to the ground and excited states of TcO_4^-. For the ground state, the electron correlation works to relax the ionicity of the M–O bond. For the excited states, the observed three absorption peaks in the electronic spectrum are assigned to the lower three dipole-allowed $^1T_2$ states. Further, the existence of the weak and strong peaks in the energy region higher than the observed one is predicted. The similarity and the difference in the electronic spectra of TcO_4^- and MnO_4^- are clarified. Band II in the spectrum of TcO_4^- is quite different from the corresponding band in the MnO_4^- spectrum, as seen in Fig. 1. The reason is the remarkably high energy shift of the 3^1T2 state ($1t_1 \rightarrow 4t_2$) of TcO_4^-, and is due to the larger antibonding nature of the $4t_2$ MOs of TcO_4^- than that of MnO_4^-.

References

1. Carrington A, Symmons MC (1963) Chem Rev 63:443
2. Ziegler T, Rauk A, Baerends EJ (1976) Chem Phys 16:209
3. Lee DG, Moylan CR, Hayashi T, Brauman JI (1987) J Am Chem Soc 109:3003
4. Nakai H, Nakatsuji H (1994) J Mol Struct (Theochem) 311:141
5. Jitsuhiro S, Nakai H, Hada M, Nakatsuji H (1994) J Chem Phys 101:1029
6. Nakatsuji H, Saito S (1990) J Chem Phys 93:1865
7. Nakai H, Ohmori Y, Nakatsuji H (1991) J Chem Phys 95:8287
8. Nakatsuji H, Saito S (1991) Int J Quant Chem 39:93
9. Yasuda K, Nakatsuji H (1993) J Chem Phys 99:1945
10. Nakatsuji H, Hirao K (1978) J Chem Phys 68:2035
11. Nakatsuji H (1978) Chem Phys Lett 59:362; (1979) Chem Phys Lett 67: 329, 334
12. Nakatsuji H (1992) Acta Chim Hung 129:719
13. Colton R, Peacock RD (1962) Quart Rev Chem Soc 16:299
14. Mullen P, Schwochau K, Jørgensen CK (1969) Chem Phys Lett 3:49

15. Krebs B, Hasse KD (1976) Acta Cryst B32:1334
16. Huzinaga S, Andzelm J, Klobukowski M, Radzio-Andzelm E, Sakai E, Tatewaki H (1984) Gaussian basis set for molecular calculations. Elsevier, New York
17. Dupuis M, Farazdel A (1991) MOTECC-91; Center for Scientific and Engineering Computations, IBM Corporation
18. Nakatsuji H (1985) Program system for SAC and SAC-CI calculations, Program Library No 146 (Y4/SAC), (1981) Data Processing Center of Kyoto University; Program Library SAC85 No 1396, Computer Center of the Institute for Molecular Science
19. Nakatsuji H (1983) Chem Phys 75:425
20. Johnson LW, McGynn SP (1970) Chem Phys Lett 7:618
21. Johnson LW, Hughes E, McGynn SP (1971) J Chem Phys 35:4476